

Water-Dispersible Nanocatalysts with Engineered Structures: The New Generation of Nanomaterials for Energy-Efficient CO₂ Capture

Masood S. Alivand, Omid Mazaheri, Yue Wu, Ali Zavabeti, Geoffrey W. Stevens, Colin A. Scholes, and Kathryn A. Mumford*



Cite This: *ACS Appl. Mater. Interfaces* 2021, 13, 57294–57305



Read Online

ACCESS |

Metrics & More

Article Recommendations

Supporting Information

ABSTRACT: The high energy demand of CO₂ absorption–desorption technologies has significantly inhibited their industrial utilization and implementation of the Paris Climate Accord. Catalytic solvent regeneration is of considerable interest due to its low operating temperature and high energy efficiency. Of the catalysts available, heterogeneous catalysts have exhibited relatively poor performances and are hindered by other challenges, which have slowed their large-scale deployment. Herein, we report a facile and eco-friendly approach for synthesizing water-dispersible Fe₃O₄ nanocatalysts coated with a wide range of amino acids (12 representative molecules) in aqueous media. The acidic properties of water-dispersible nanocatalysts can be easily tuned by introducing different functional groups during the hydrothermal synthesis procedure. We demonstrate that the prepared nanocatalysts can be used in energy-efficient CO₂ capture plants with ease-of-use, at very low concentrations (0.1 wt %) and with extra-high efficiencies (up to ~75% energy reductions). They can be applied in a range of solutions, including amino acids (i.e., short-chain, long-chain, and cyclic) and amines (i.e., primary, tertiary, and primary-tertiary mixture). Considering the superiority of the presented water-dispersible nanocatalysts, this technology is expected to provide a new pathway for the development of energy-efficient CO₂ capture technologies.

KEYWORDS: water-dispersible nanocatalyst, energy-efficient CO₂ capture, amino acids, acidic Fe₃O₄ surface functionalization



1. INTRODUCTION

Anthropogenic CO₂ emission is recognized as a major contributor to global warming and climate change.^{1,2} Clear gaps between high energy demands and accessible supplies of energy show that fossil fuels (e.g., coal, natural gas, and crude oil) will likely remain the primary energy source until 2050.^{3,4} This future pathway is of concern as fossil fuel use comprises a significant portion of the overall CO₂ emission portfolio.⁵ Considering the low price of fossil fuels and the key role of coal-fired power plants in electricity generation, international attempts (e.g., Paris Agreement) have not yet been successful in harnessing global temperature rise. Hence, postcombustion CO₂ capture can be considered as the best techno-economical methodology available to exploit the energy of fossil fuels while controlling their detrimental environmental impacts.^{6,7}

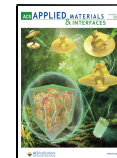
Among different CO₂ capture techniques, like absorption,^{8,9} adsorption,^{10,11} cryogenic distillation,^{12,13} and membrane separation,^{14,15} chemical absorption using aqueous amine solutions, particularly monoethanolamine (MEA), has attracted great attention as a mature technology for large-scale operations.¹⁶ Nevertheless, the energy-intensive nature of CO₂ absorption–desorption processes markedly impacts the costs of operation, creating a solid barrier to its widespread deployment in different industries.^{17,18} This drawback is

mainly due to the slow kinetics of CO₂ desorption reactions in the solvent regeneration process. A high operating temperature of 120–140 °C is usually applied to compensate for the slow rate of CO₂ desorption, which remarkably increases the cost of operation.¹⁹ Therefore, energy-efficient CO₂ absorption–desorption techniques (e.g., using new and blended amines, amino acid solutions, phase-change solvents and liquid nanoabsorbents) have been of great interest.^{20,21} Catalytic solvent regeneration is a recently emerged energy-efficient method to accelerate the kinetics of CO₂ desorption and enable solvents to be regenerated below 100 °C, much lower than their typical boiling points.²² This lower operating temperature not only avoids the loss of the latent heat of vaporization, it also paves the way for hot water streams from green and renewable energy resources (e.g., solar hot water) or those already available in the processes (e.g., hot process water

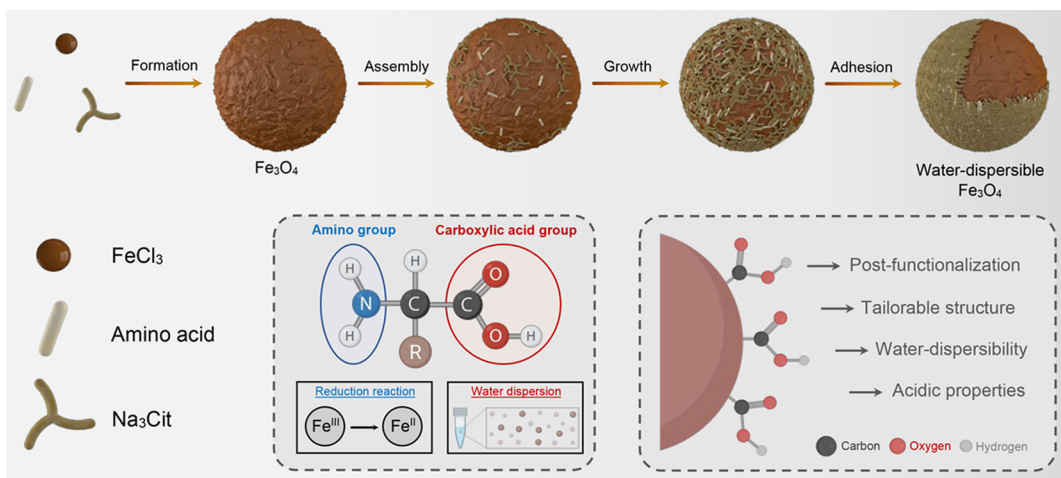
Received: September 13, 2021

Accepted: November 15, 2021

Published: November 23, 2021



Scheme 1. Synthesis strategy for preparing water-dispersible Fe_3O_4 using amino acids. The presence of amino groups allows for the conversion of Fe^{III} to Fe^{II} through a one-pot hydrothermal synthesis methodology, while the acidic functional groups result in the hydrophilic property of water-dispersible nanomaterials and their proton donation ability in the catalytic reactions



streams) to be used for solvent regeneration, thereby significantly reducing operating costs.

Throughout the past decade, a broad span of heterogeneous solid acid catalysts ranging from metal-oxides (e.g., ZnO^{23} and MoO_3^{24}) to nanoporous materials (e.g., modified montmorillonite²⁵ and HZSM-5 zeolite²⁶) and nanocomposites (e.g., Fe promoted $\text{SO}_4^{2-}/\text{ZrO}_2/\text{MCM}-41^{27}$ and $\text{SO}_4^{2-}/\text{ZIF}-67-\text{C}@\text{TiO}_2^{28}$) have been tested in catalyst-aided solvent regeneration processes. Despite intensive research and development efforts, industrial-scale uptake of catalytic solvent regeneration technology has not been widely adopted due to the drawbacks of heterogeneous catalysis, such as operating challenges and low efficiency in the liquid phase. More importantly, high performing heterogeneous nanocomposites require complex synthesis procedures, particularly when an engineered porosity or functionalized surface is required, making them expensive options. Hence, it is of considerable importance to investigate the potential of advanced nanomaterials with facile and inexpensive preparation methodologies, engineered structures and targeted physicochemical merits.^{29–31}

Herein, we report a facile and eco-friendly strategy for synthesizing highly water-dispersible Fe_3O_4 nanocatalysts with abundant acidic sites and tunable structures. The experimental results show that the presence of amino acids, containing both amino (i.e., $-\text{NH}_2$) and carboxyl (i.e., $-\text{COOH}$) functional groups, in the aqueous medium enables the partial reduction of Fe^{III} to Fe^{II} , producing carboxylate-stabilized Fe_3O_4 nanomaterials with unique properties (Scheme 1). The assembly of carboxylates on the exterior surface of Fe_3O_4 also makes it a versatile platform for subsequent surface functionalization, thus allowing for enrichment with stronger acidic sites (e.g., $-\text{SO}_3\text{H}$). The unique combination of physical (i.e., the nanofluidic behavior) and chemical (i.e., proton donation ability of acidic groups) promotion effects, enables the resulting water-dispersible nanomaterials to effectively participate in solvent regeneration reactions and enhance CO_2 desorption at low operating temperatures with reduced energy consumption. The simplicity of CO_2 capture processes when using water-dispersible nanocatalysts, as well as its compatibility with renewable energy resources for cyclic operation,

makes this technology a new approach for advanced catalytic solvent regeneration.

2. EXPERIMENTAL SECTION

2.1. Materials. All amino acids, ferric ammonium citrate, 3-(*n*-morpholino)propanesulfonic acid (MOPS, >99.5%), 4-dorpholineethanesulfonic acid (MES, 99.5%), monoethanolamine (MEA, >99.5%), *n*-methyldiethanolamine (MDEA, >99.0%), and sulfanilic acid (99.0%) were reagent grade and purchased from Sigma-Aldrich. Ethanol (>99.5%), acetone (>99.5%), and potassium hydroxide (KOH, >85.0%) were purchased from Chem-Supply, Australia. 1-Ethyl-3-(3-(dimethylamino)propyl) carbodiimide hydrochloride (EDC, 99%) and *N*-hydroxysuccinimide (NHS, 99%) were obtained from Proteochem, USA. Ultrapure nitrogen (N_2 , 99.9%) and carbon dioxide (CO_2 , 99.9%) were supplied by BOC Gases Australia and used for CO_2 absorption-desorption experiments.

2.2. Preparation of Water-Dispersible Fe_3O_4 Nanocatalysts. For the synthesis of water-dispersible Fe_3O_4 nanocatalysts, 20 mmol of ferric ammonium citrate and 150 mmol of amino acid were dissolved in 100 mL water under vigorous stirring at room temperature. Then, the pH was raised to 11 by adding 10 M potassium hydroxide solution, changing the color from dark to reddish-brown. The solution was transferred to a stainless-steel autoclave and heated at 200 °C for 8 h. Afterward, the autoclave was gradually cooled to room temperature and black solid precipitates were separated via the application of an external magnet. The obtained nanomaterials were repeatedly washed with acetone, ethanol and water to remove unreacted or physically attached molecules. During each washing step, the prepared products were suspended in the solvent, ultrasonicated for 30 min and separated by an external magnet. Finally, the resultant materials were dried at 75 °C overnight under severe vacuum and labeled as $\text{Fe}_3\text{O}_4-\text{X}$, where X denotes the name of the amino acid used during the hydrothermal synthesis of water-dispersible nanocatalyst. For instance, $\text{Fe}_3\text{O}_4-\text{Ala}$ and $\text{Fe}_3\text{O}_4-\text{His}$ represent the water-dispersible nanomaterials prepared with Alanine and Histidine, respectively. The abbreviation used for amino acids along with their molecular structures is illustrated in Figure S1.

2.3. Postfunctionalization of Acid-Wrapped Fe_3O_4 Nanomaterials. The preprepared water-dispersible nanomaterials were postfunctionalized by the EDC-NHS cross-linking method in two steps. First, the acidic Fe_3O_4 nanomaterials were functionalized by amine-reactive NHS molecules. Typically, 1 g of preprepared Fe_3O_4 with acid functional groups was first dispersed in MES buffer solution (500 mL, 0.1 M, pH 5.5) and sonicated for 30 min to completely disperse nanomaterials in the solution. After stirring for 4 h at room

temperature, EDC (1.6 g) and NHS (1.0 g) were added and the solution was stirred for 6 h. The amine-reactive nanomaterials were subsequently separated using an external magnet and washed several times with water to remove unreacted EDC/NHS molecules. The second step involved the surface functionalization of acid-wrapped Fe_3O_4 using a molecule containing both amine (to react on the surface) and the targeted functional group (e.g., $-\text{SO}_3\text{H}$). Considering the main focus of this research is on acidic nanomaterials, sulfanilic acid was chosen as the desired molecule. Briefly, EDC-NHS activated Fe_3O_4 nanomaterials were subsequently redispersed in MOPS buffer (400 mL, 0.1 M, pH 7.5) and sonicated for 30 min. The cross-linking reaction started by introducing sulfanilic acid solution (100 mL, 1 M) and proceeded for 1 h under continuous stirring. The resulting nanomaterials were separated, washed with water three times, and dried at 75 °C under vacuum overnight.

2.4. Characterization. Fourier-transform infrared (FTIR) spectra were measured using a Bruker Tensor II in 400–4000 cm^{-1} range. X-ray photoelectron spectroscopy (XPS) was conducted on a VG ESCALAB 220i-XL spectrometer with A1 $\text{K}\alpha$ radiation and 1486.6 eV photon energy. Thermogravimetric analysis (TGA) was performed on a NETZSCH TG 209 F1 Libra analyzer in 30–800 °C range with 10 °C/min heating rate in N_2 atmosphere. The ζ potential was measured by a Malvern Zetasizer Nano ZS. Scanning electron microscopy (SEM) was performed on a FEI Teneo instrument with an operating voltage of 20 kV. Before taking SEM images, the materials were sputtered with 10 nm gold by a Quorum K575X ion sputter instrument with 30 mA current. Transmission electron microscopy (TEM), high-angle annular dark-field (HAADF) imaging, energy-dispersive X-ray spectroscopy (EDX) mapping and line spectra analysis were carried out on a JEOL 2100f instrument with a 200 kV acceleration voltage, equipped with oxford X-MaxN 80T detector and Gatan OneView 4k camera.

2.5. CO_2 Capture Experiments. Both CO_2 absorption and desorption experiments were conducted in an in-house modified OptiMax workstation 1001 (Mettler-Toledo) connected to a dynamic gas flow apparatus (Figure S2). The device was equipped with a 1000 mL reactor, an adjustable mixer to keep the solution uniform, and a temperature controller system including a thermocouple and a heating jacket vessel to accurately control the reactor operating temperature and measure heat transfer parameters.

In a typical CO_2 absorption experiment, 500 mL of preprepared aqueous solution and 0.1 wt % of water-dispersible nanocatalyst were mixed. The prepared solution was sonicated for 30 min at 60 °C and then transferred to the reactor. To mimic the operating conditions of CO_2 absorption from postcombustion flue gas streams, the reactor temperature, pressure and rotation speed were set at 40 °C, 40 kPag and 400 rpm, respectively. Then, a constant flow of a CO_2/N_2 binary mixture (635 mL/min, 10 vol % CO_2 and 90 vol % N_2) was bubbled into the solvent. For this purpose, two separate gas flow controllers were utilized to provide constant CO_2 (Aalborg, CO₂-GFC17, 0–100 mL/min) and N_2 (Aalborg, N₂-GFC17, 0–10 L/min) streams. The treated gas stream was cooled using a Graham condenser connected to an external water circulator (-2 ± 0.1 °C) and the evaporated solvent returned to the reactor. The gas was then passed through two consecutive ice bath condensers (acetone–water mixture with -15 ± 5 °C) to ensure any remaining moisture was trapped. The concentration of CO_2 and the volumetric flow rate of the treated gas stream were measured using an online CO_2 analyzer (BlueSens, BCP-CO₂) and a digital flow meter (Aalborg, GFM17, 0–1000 mL/min), respectively. During the CO_2 absorption experiment, the concentration of CO_2 in the outlet stream was regularly monitored and the binary gas flow stopped bubbling when the concentration of CO_2 at outlet stream reached 15 ± 0.1 vol %.

For CO_2 desorption experiments, N_2 gas was used as the carrier gas at a flow rate of 90 mL/min. The CO_2 desorption process started by increasing the reactor temperature from 40 to 88 °C, maintaining this temperature for 30 min and then finished by returning the temperature to 40 °C. To quantitatively perform heat flow calorimetry analysis and measure the amount of energy consumed during the catalyst-aided solvent regeneration, the OptiMax workstation was

connected to the OptiMax HFCal (Mettler-Toledo) probe. iControl software was used to directly record and evaluate all information received by the OptiMax workstation and HFCal. Once the solvent regeneration finished, the reactor operating temperature was maintained at 40 °C and the N_2 inlet valve closed. Solvent samples were taken and the next CO_2 absorption–desorption cycle initiated.

To test the reliability of data measured by the online CO_2 analyzer, the CO_2 loading of the aqueous amine solution was also measured by CO_2 Coulometer equipment (CMS015) with ± 0.01 mol/L accuracy connected to an internal acidification module (CMS230). For each measurement, 2 mL CO_2 -loaded amine solution was titrated using 1 mL of concentrated H_2SO_4 to release captured CO_2 molecules. The comparative results of CO_2 loading using gas and liquid measurement techniques are presented in Figure S3 confirming the reliability of the quantitative CO_2 absorption–desorption measurement technique used in this study.

The flow rate of desorbed CO_2 was calculated using the following eq (eq 1):

$$n_{\text{CO}_2} = \frac{X_{\text{CO}_2}}{1 - X_{\text{CO}_2}} n_{\text{N}_2} \quad (1)$$

where n_{CO_2} (mol/min) is the flow rate of CO_2 at outlet stream, n_{N_2} (mol/min) is the flow rate of N_2 at outlet stream and in the volume fraction of CO_2 in CO_2/N_2 binary mixture detected by the CO_2 analyzer.

The total amount of released CO_2 (N_{CO_2} , mol) during the solvent regeneration process (t , min) was calculated by the following eq (eq 2):

$$N_{\text{CO}_2} = \int_0^t n_{\text{CO}_2} dt \quad (2)$$

The heat duty (HD, kJ/mol) of CO_2 desorption operation was calculated by the following eq (eq 3):

$$\text{HD} = \frac{E}{N_{\text{CO}_2}} \quad (3)$$

where E (kJ) is the amount of consumed energy calculated according to the following eq (eq 4):

$$E = \int_0^t \text{HF} dt \quad (4)$$

where HF (kW) is the heat flow measured by the HFCal probe.

To compare the efficiency of different heterogeneous catalysts, relative heat duty (RH, %) was calculated by the following eq (eq 5):

$$\text{RH} = \frac{\text{HD}_{\text{cat}}}{\text{HD}_{\text{Blank}}} \times 100 \quad (5)$$

where HD_{cat} (kJ) is the heat duty required for the solvent regeneration process in the presence of catalyst and HD_{blank} (kJ) is the amount of required energy for the regeneration of the blank solvent without any catalysts.

3. RESULTS AND DISCUSSION

3.1. Preparation of Hydrophilic Fe_3O_4 Nanocatalysts.

The primary benefit of the reported synthesis methodology is that the acid-wrapped Fe_3O_4 nanomaterials can be obtained simply by a one-pot synthesis route in the aqueous solution without any postfunctionalization required. Additionally, both ferric ammonium citrate and amino acids are environment-friendly and low-cost chemicals, making the fabrication of water-dispersible nanocatalysts an affordable process and enabling its large-scale utilization in various industries. To examine the applicability of our synthesis methodology to various amino acids, a broad range of amino acids were used during the hydrothermal synthesis of acid-wrapped Fe_3O_4 nanocatalysts. The FTIR spectra of all prepared Fe_3O_4 samples

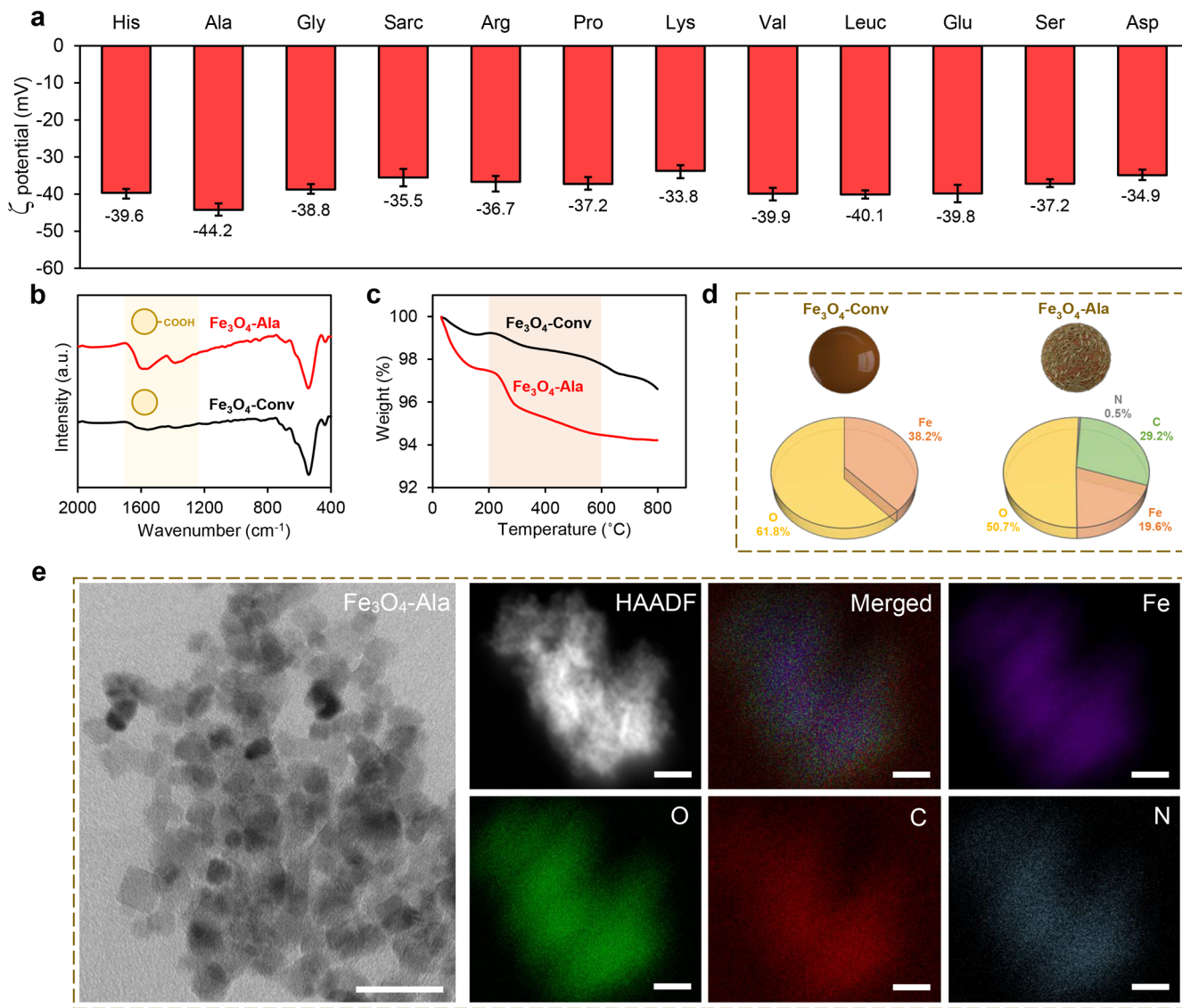


Figure 1. Analysis of water-dispersible Fe_3O_4 nanoparticles. (a) ζ potential values of various water-dispersible Fe_3O_4 nanomaterials prepared using different amino acids (all nanomaterials were dispersed in 0.1 M MOPS buffer at pH 9.0). (b) FTIR spectra, (c) TGA curves under a nitrogen atmosphere, and (d) XPS analysis of conventional Fe_3O_4 prepared via the coprecipitation method ($\text{Fe}_3\text{O}_4\text{-Conv}$) and $\text{Fe}_3\text{O}_4\text{-Ala}$ as the representative of water-dispersible nanomaterials. (e) TEM image, HAADF, and EDX elemental mapping of $\text{Fe}_3\text{O}_4\text{-Ala}$. Scale bars are 20 nm in the TEM image and 50 nm in HAADF and EDX images.

were similar to three characteristic peaks (Figures S4 and S5). The sharp peak at $\sim 550 \text{ cm}^{-1}$ is associated with the Fe—O vibration of the Fe_3O_4 structure.³² Two peaks at ~ 1340 and $\sim 1610 \text{ cm}^{-1}$ are ascribed to the C=O and C—O stretching of the carboxylic acid group, coming from amino acid and trisodium citrate molecules.³³ Furthermore, all the Fe_3O_4 nanoparticles had a negative surface ζ potential, ranging from -33.8 (i.e., $\text{Fe}_3\text{O}_4\text{-Lys}$) to -44.2 mV (i.e., $\text{Fe}_3\text{O}_4\text{-Ala}$), indicating the accumulation of carboxylic acid groups on the exterior surface of Fe_3O_4 particles (Figure 1a). In detail, the deprotonation of carboxylic acid groups in a basic medium (MOPS buffer, pH 9.0) creates negatively charged ions on the surface of the nanoparticle, resulting in highly negative ζ potential values.

The importance of the amino acids in the structural formation of Fe_3O_4 was examined by changing the amount of amino acid during hydrothermal synthesis. By increasing the amount of amino acid, the color of the synthesized

nanomaterials changed from reddish-brown to dark black, suggesting the formation of Fe_2O_3 (only composed of Fe^{III}) and Fe_3O_4 (composed of both Fe^{III} and Fe^{II}) materials, respectively. It should be noted that using amino acids in the initial solution was imperative to achieve the final Fe_3O_4 product. This confirms the critical role of amino acid in the partial reduction of Fe^{III} to Fe^{II} in the aqueous solution, which is necessary for the formation of Fe_3O_4 nanoparticles. Among all types of amino acids used, we selected alanine (Ala) as a model amino acid for further experiments, owing to its simple structure, availability, and the lowest ζ potential value among all synthesized Fe_3O_4 nanoparticles.

Different characterization methods were used to compare the structural properties of our synthesized $\text{Fe}_3\text{O}_4\text{-Ala}$ nanomaterials with those of the conventional Fe_3O_4 ($\text{Fe}_3\text{O}_4\text{-Conv}$) obtained by the coprecipitation method. FTIR spectroscopy revealed that the position of the Fe—O peak is the same in both samples, while $\text{Fe}_3\text{O}_4\text{-Ala}$ exhibited the

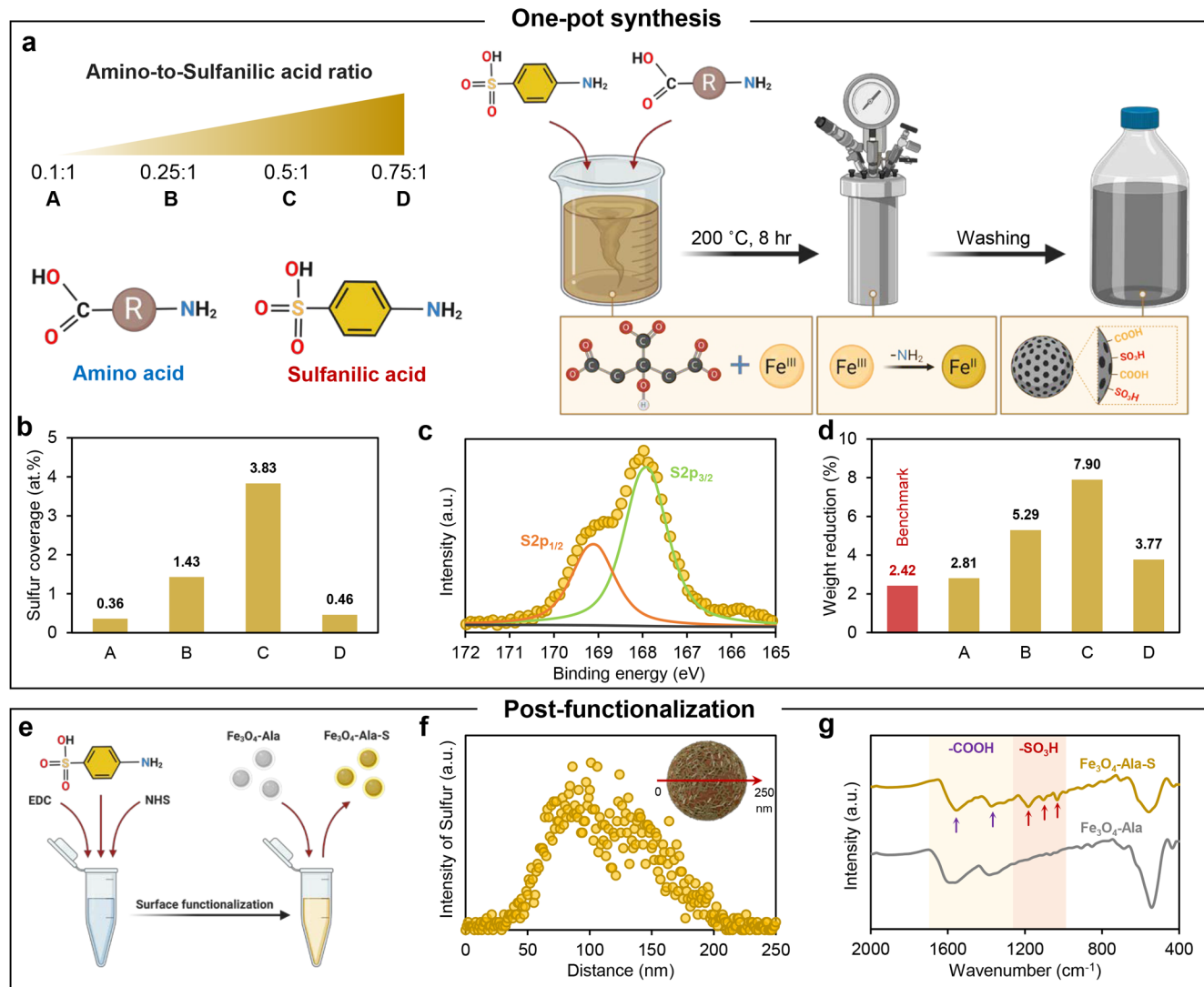


Figure 2. Engineering the acidity of water-dispersible Fe_3O_4 nanomaterials. (a) Schematic of the surface engineering of water-dispersible nanocatalysts by adjusting amino-to-sulfanilic acid ratio during one-pot synthesis methodology. The benchmark stands for Fe_3O_4 -Ala without surface engineering, and the prepared materials were labeled using the alphabet associated with their amino-to-sulfanilic acid ratio. For example, A represents the Fe_3O_4 -Ala-A sample with an amino-to-sulfanilic acid ratio of 0.1:1. (b) The amount of sulfur (detected by XPS), (c) the nature of sulfur functional groups (detected by XPS), and (d) the total amount of functional groups (measured by TGA in nitrogen) on the surface of engineered water-dispersible nanocatalysts. (e) Schematic of the surface functionalization of Fe_3O_4 -Ala using EDC/NHS cross-linking agents (i.e., Fe_3O_4 -Ala-S). (f) The intensity of sulfur elements through the structure of postfunctionalized Fe_3O_4 -Ala-S (detected by sulfur line scanning). (g) FTIR spectra of Fe_3O_4 -Ala and Fe_3O_4 -Ala-S nanocatalysts.

characteristic peaks of carboxylic acid at around ~ 1340 and $\sim 1610 \text{ cm}^{-1}$ (Figure 1b). To quantitatively measure the amount of acidic functional groups, TGA was performed under a N_2 flow, and the weight reduction of samples between 250 and 600°C was used as an indicator of acidic functional groups, including both carboxylic acids and hydroxyl groups (Figure 1c).³³ The results revealed that Fe_3O_4 -Ala (2.4 wt % reduction) had $\sim 70\%$ more acidic functional groups than that of Fe_3O_4 -Conv (1.4 wt % reduction).

The exterior surface of Fe_3O_4 -Ala was further analyzed by XPS characterization, which showed the presence of carbon (~ 29.2 at %) on the exterior surface of Fe_3O_4 -Ala (Figure 1d; see also Figure S6). This could be attributed to the assembly of citrate ions and amino acid molecules to the metal-oxide surface due to their strong adhesion at high synthesis temperatures.³⁴ Notably, Fe_3O_4 -Ala displayed negligible

nitrogen on the surface (~ 0.5 at %), which may be due to the degradation of amino acid molecules at high temperatures and weak covalent interaction of amine groups to the surface. Comparatively, Fe and O were the only elements on the surface of Fe_3O_4 -Conv, confirming the modified structure of Fe_3O_4 -Ala. SEM and TEM images also showed that Fe_3O_4 -Ala has a regular morphology with small semicubic particles in the range of ~ 5 – 20 nm (Figures 1e and S7). HAADF and EDX mapping results revealed the presence of Fe, O, C, and N elements with homogeneous distribution through the Fe_3O_4 -Ala structure. The detected N by the TEM-EDX technique was considerably greater than that of XPS, which can signal higher concentrations of N in the structure of Fe_3O_4 -Ala, rather than its external surface.

The suggested hydrothermal approach for the one-pot synthesis of acid-wrapped Fe_3O_4 nanomaterials can make it a

good option in a broad range of industrial applications. The coating layer derived from carboxyl-containing molecules (i.e., trisodium citrate and amino acid) significantly enhances the hydrophilicity of the metal-oxide substrate, enabling the synthesized Fe_3O_4 to effectively be used for the preparation of magnetic metal-oxide nanofluids (Figure S8).³⁵ The hydrophilicity of Fe_3O_4 -Ala was evaluated by mixing its aqueous solution with various organic solvents, including ethyl acetate, cyclohexane, 1, 2-dichloroethane, and dichloromethane (DCM) (Figure S9). After full dispersion into the binary solvents, Fe_3O_4 -Ala nanomaterials accumulated in the aqueous phase after a short relaxation time in all studied mixtures. In addition to the hydrophilic nature of Fe_3O_4 -Ala and its nanofluidic properties in the aqueous solution, the acidic coating on the metal-oxide surface endows the Fe_3O_4 -Ala with excellent proton donation capability and catalytic properties for energy-efficient CO_2 capture. The water-dispersible nanocatalysts can also show great potential for many different industrial applications. For example, for the large-scale production of bio-oil and biodiesel from the pyrolysis of cellulose and algae, Fe_3O_4 -Ala can govern the esterification reaction in the aqueous phase, while the catalysts remain in the water phase, owing to their hydrophilicity, and a pure oily phase can be continuously produced.³⁶

3.2. Engineering the Acidic Characteristics of Fe_3O_4 -Ala. As the carboxyl functional group is the main source of Brønsted acid sites in Fe_3O_4 -Ala nanocatalysts, using stronger Brønsted acid groups can markedly improve catalytic properties. Hence, we used sulfanilic acid as an organic compound with both amino and sulfo groups in its molecular structure. To examine the role of sulfanilic acid during the synthesis of Fe_3O_4 -Ala, a series of nanomaterials with different amino-to-sulfanilic acid ratios (i.e., 0.1:1 (A), 0.25:1 (B), 0.5:1 (C), and 0.75:1 (D)) were synthesized (Figure 2a). It is worth noting that no final product was obtained by substituting amino acid with sulfanilic acid, reconfirming the critical role of amino acids in the reduction of Fe^{III} to Fe^{II} during the formation of Fe_3O_4 structure in the aqueous solution.

The effect of amino-to-sulfanilic acid ratio variation on the surface of the prepared nanomaterials was investigated using XPS. As shown in Figure 2b, increasing the amino-to-sulfanilic acid ratio led to an increase in the amount of sulfur on the surface of Fe_3O_4 -Ala, changing from 0.36 at % in Fe_3O_4 -Ala-A to 3.83 at % in Fe_3O_4 -Ala-C. This is mainly due to the importance of amino acids in the formation reaction of Fe_3O_4 , which caused a well-defined crystalline structure and provided more sites for the assembly of sulfate groups onto the surface. However, when the amino-to-sulfanilic acid ratio increased to 0.75:1 in Fe_3O_4 -Ala-D, the amount of sulfur remarkably reduced to 0.46 at %, indicating the competition between amino acid and sulfanilic acid and the poor performance of the sulfation process at high concentrations of amino acids. In the XPS high-resolution S 2p spectrum of Fe_3O_4 -Ala-C, the binding energies at 168.7 (i.e., S 2p_{3/2}) and 169.1 eV (i.e., S 2p_{1/2}), which were ascribed to S-OH and S=O, respectively, confirm the presence of $-\text{SO}_3\text{H}$ groups as the main source of sulfur on the surface of nanomaterials (Figure 2c).³⁷ Notably, we could not observe any significant changes in the shape and size of engineered Fe_3O_4 -Ala-A/D nanocatalysts (Figure S10), revealing the negligible effect of amino-to-sulfanilic acid ratio on the morphology of water-dispersible nanocatalysts.

To further understand the influence of amino-to-sulfanilic acid ratio on the functional groups of Fe_3O_4 nanocatalysts, the

weight reduction of Fe_3O_4 -Ala-A to -D was measured using TGA in 250–600 °C range and compared with Fe_3O_4 -Ala as the benchmark (Figure 2d). A similar trend was observed between the total functional groups of modified materials via the TGA and sulfur content from XPS, in which Fe_3O_4 -Ala-C exhibited the maximum acidic functional groups of 7.9 wt % (more than two times greater than that of Fe_3O_4 -Ala). From these observations, it is proposed that the amino-to-sulfanilic acid ratio can be used as a key parameter to engineer the structure of water-dispersible nanocatalysts and their acidic properties.

Besides tuning the functional layer of Fe_3O_4 -Ala by simply varying the ratio of acidic components during one-pot synthesis methodology, the applicability of postfunctionalization was also explored. For this purpose, Fe_3O_4 -Ala nanomaterials were dispersed in EDC-NHS solution, followed by introducing sulfanilic acid containing both amino (to react with the amine-reactive surface of EDC-NHS activated Fe_3O_4 -Ala) and sulfo (as the targeted functional group with excellent proton donation ability) groups (Figure 2e). After cross-linking of Fe_3O_4 -Ala surface via sulfanilic acid (i.e., Fe_3O_4 -Ala-S), the obtained nanomaterials were characterized. EDX line scanning revealed the presence of a S element on the surface of Fe_3O_4 -Ala-S with a uniform distribution (Figure 2f). In addition, the FTIR spectrum of Fe_3O_4 -Ala-S showed the appearance of S=O and S—O stretching in the ~1000–1200 cm⁻¹ range, while the vibrations associated with the carboxylic acid groups did not display a significant change compared to those of Fe_3O_4 -Ala, confirming the successful sulfation of Fe_3O_4 -Ala through a post surface functionalization method (Figure 2g).^{37,38} The facile surface functionalization of Fe_3O_4 -Ala in the aqueous medium provides further versatility for engineering its acidic characteristics using various functional groups (e.g., —PO₃H and —SH) in future studies.

3.3. Catalytic CO_2 Desorption Performance. To demonstrate that the water-dispersible Fe_3O_4 nanomaterials can be used as the new generation of acidic nanocatalysts, we designed a new process configuration for a CO_2 absorption-desorption process, which is compatible with the structure of water-dispersible nanocatalysts. During the typical CO_2 desorption process, the temperature of the solvent increases up to and beyond its boiling point (i.e., ~120–140 °C depending on the solvent and operating pressure of the column) to provide enough activation energy for CO_2 desorption reactions.²² The required energy at high temperatures is usually provided by medium-high pressure steam passing through a reboiler in the bottom of the regeneration column.³⁹ In addition to the expensive cost of steam, a large quantity of the required energy (up to ~50%) is wasted by the latent heat of solvent evaporation.^{40,41} This problem may be addressed using heterogeneous catalysts, in which the solvent can be regenerated at a temperature less than its boiling point, and a steam reboiler can be substituted with a liquid–liquid heat exchanger operating with hot water to regenerate the CO_2 -rich solvent. However, there still remains a need to use a desorption column as a medium to load heterogeneous solid acid catalysts and provide enough contact area between liquid and catalyst interface. In contrast, our presented water-dispersible nanocatalysts can be directly dispersed and stored in the liquid phase, owing to their high stability in various aqueous solvents (see Figure S11). Accordingly, the regeneration column has been omitted in the new process design and

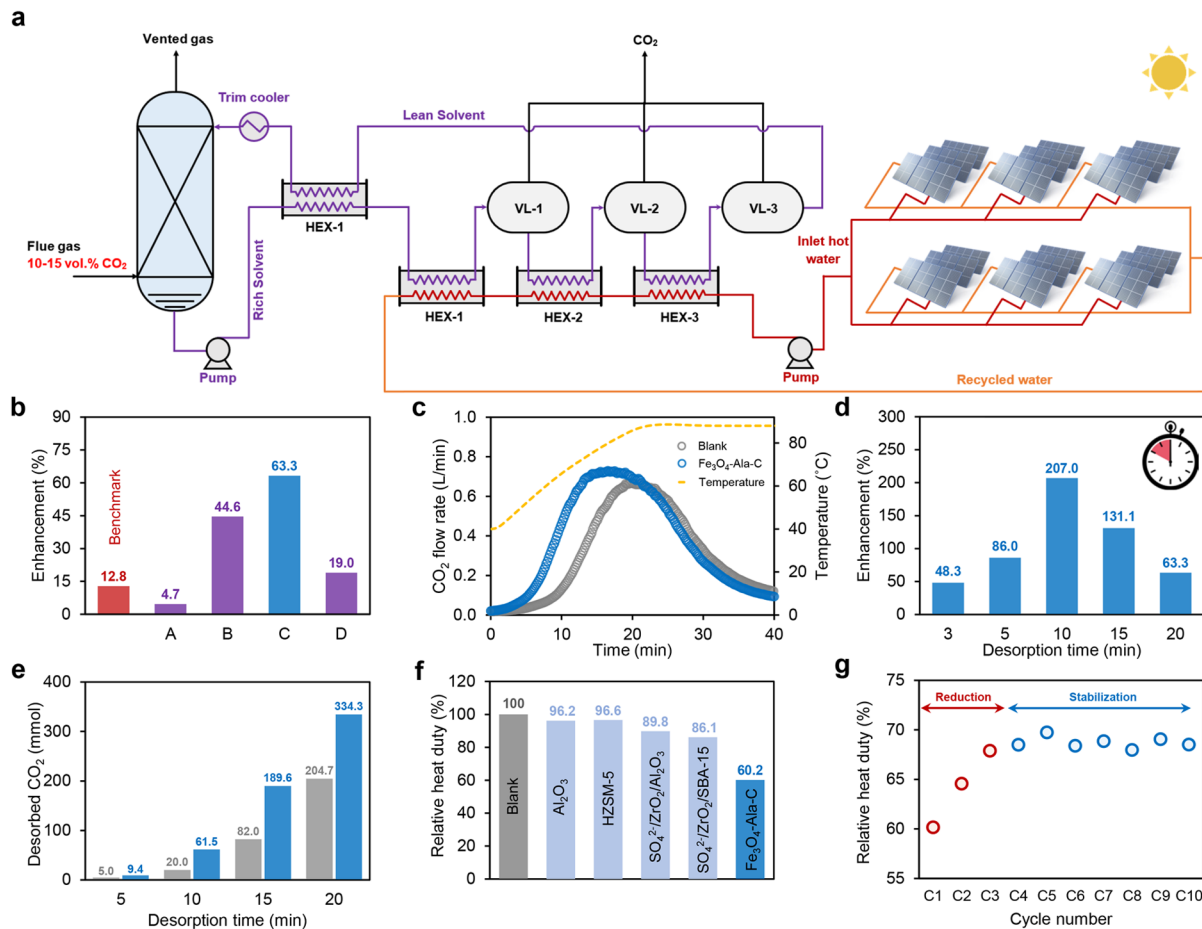


Figure 3. Low-temperature CO_2 desorption performance of water-dispersible nanocatalysts. (a) The schematic diagram of the large-scale cyclic CO_2 absorption–desorption process, particularly designed for a compatible operation with water-dispersible nanocatalysts and solar hot water as the main source of energy for low-temperature solvent regeneration. (b) The CO_2 desorption enhancement of 5 M MEA solution in the presence of different engineered water-dispersible nanocatalysts, compared to that of the blank solution without using any nanocatalyst. Panels A to D represent Fe_3O_4 -Ala-A–D samples, respectively, and Fe_3O_4 -Ala was used as the benchmark. (c) The CO_2 desorption and regeneration temperature profiles of 5 M MEA solution without (blank) and in the presence of a Fe_3O_4 -Ala-C nanocatalyst. (d) The CO_2 desorption enhancement and (e) the total amount of desorbed CO_2 at different time intervals during the catalytic regeneration of 5 M MEA solution using a Fe_3O_4 -Ala-C nanocatalyst. (f) The relative heat duty of 5 M MEA solution in the presence of heterogeneous catalysts (Al_2O_3 metal oxide, HZSM-5 zeolite, SO_4^{2-} / ZrO_2 / Al_2O_3 , and SO_4^{2-} / ZrO_2 /SBA-15 composites) and a water-dispersible Fe_3O_4 -Ala-C nanocatalyst. (g) The catalytic performance of Fe_3O_4 -Ala-C during consecutive CO_2 absorption–desorption cycles. The concentration of catalyst was kept constant at 0.1 wt % in all experiments.

replaced with three consecutive vapor–liquid separators working at different operating temperatures (Figure 3a).

In this design, hot water has been considered as the main source of energy at 98 °C, which can be provided from sustainable energy resources, particularly solar hot water. In addition, a constant value of 10 °C has been assumed as the effective approach temperature for all liquid–liquid heat exchangers, increasing the solvent temperature from 40 °C (i.e., absorption column temperature) to a maximum of 88 °C at the end of the liquid–liquid heating process. Therefore, 88 °C has been considered as the maximum regeneration temperature during lab-scale CO_2 desorption experiments to mimic the large-scale operation. Moreover, three vapor–liquid stages, rather than only using a single-stage, have been suggested to improve the heat transfer and, subsequently, CO_2 desorption efficiency. Nonetheless, this technology is in its early stages, and more investigations are needed to find the optimum design of CO_2 absorption–desorption units using water-dispersible nanocatalysts.

To investigate the catalytic activity of different engineered Fe_3O_4 nanocatalysts, the CO_2 desorption performance of CO_2 -rich 5 M MEA solution without using a nanocatalyst (i.e., blank) in the presence of Fe_3O_4 -Ala (i.e., benchmark) and various engineered Fe_3O_4 nanocatalysts was examined. The concentration of the water-dispersible nanocatalyst was kept constant at 0.1 wt % during all catalytic regeneration experiments. As displayed in Figure 3b, all prepared nanocatalysts with different acidic characteristics had a positive effect on the CO_2 desorption performance. Using Fe_3O_4 -Ala with only carboxylic acid groups resulted in an ~12.8% increase in the total amount of CO_2 desorbed compared to the blank solvent without any catalyst. Except for Fe_3O_4 -Ala-A with 4.7% enhancement in CO_2 desorption, all engineered Fe_3O_4 nanocatalysts exhibited a better CO_2 desorption performance than Fe_3O_4 -Ala. Specifically, the Fe_3O_4 -Ala-C nanocatalyst showed the best performance with 63.3% enhancement in total CO_2 desorbed, which is a 4-fold increase compared to the benchmark Fe_3O_4 -Ala. These findings are in

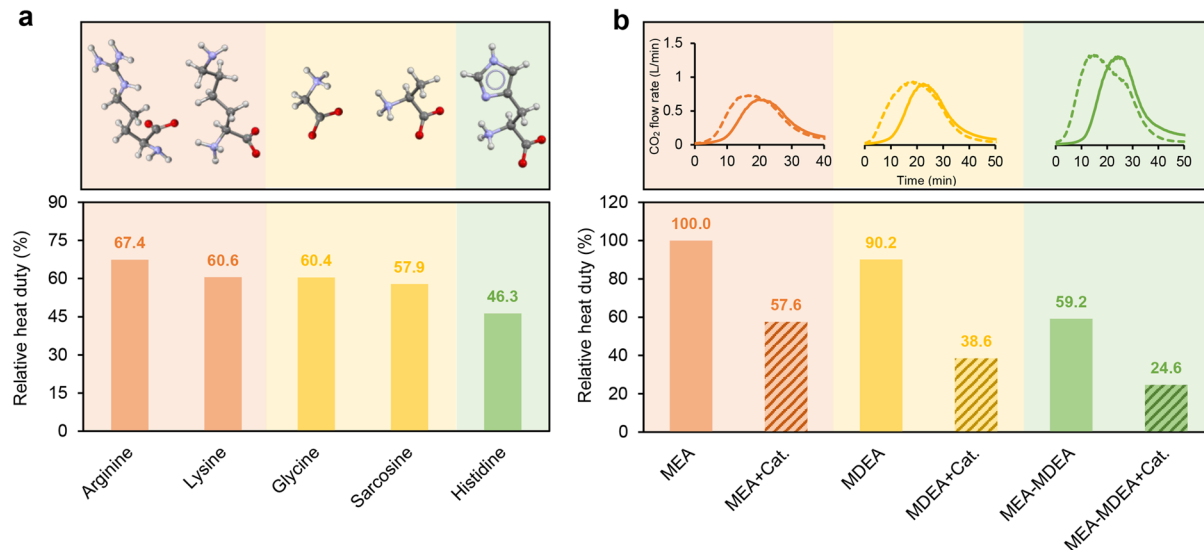


Figure 4. Versatile application of water-dispersible nanocatalysts in different aqueous solutions for energy-efficient CO_2 capture. (a) The relative heat duty of different amino acid solutions (1 M in water) in the presence of the water-dispersible Fe_3O_4 -Ala-C nanocatalyst. The relative heat duties for amino acid solutions are calculated in comparison with their corresponding heat duties without using any nanocatalyst. (b) The CO_2 desorption profile and relative heat duty primary (MEA, 5 M), tertiary (MDEA, 2 M), and primary-tertiary (MEA-MDEA, 5 M–2 M) amine solutions with and without using a water-dispersible Fe_3O_4 -Ala-C nanocatalyst. The relative heat duties for all amines are calculated in comparison with 5 M MEA solution without using a nanocatalyst. The concentration of the catalyst was kept constant at 0.1 wt % in all experiments.

line with the high density of sulfate functional groups on the surface of Fe_3O_4 -Ala-C (see section 3.2).

Next, a detailed comparison was performed between the CO_2 desorption behavior of CO_2 -saturated 5 M MEA solvent with and without Fe_3O_4 -Ala-C in the regeneration process. As seen in Figure 3c, the presence of Fe_3O_4 -Ala-C substantially facilitated CO_2 desorption from the initial moments of operation at 50 °C and increased with an increase in regeneration temperature. Although the maximum release of CO_2 in the blank solvent was achieved at the maximum temperature of ~88 °C, the solvent containing Fe_3O_4 -Ala-C nanocatalysts reached its maximum release at ~75 °C, resulting in shifting the CO_2 desorption peak from ~20 to ~16 min. Notably, the rate of CO_2 desorption started to decrease with a similar pattern in both cases when the regeneration temperature remained constant at 88 °C, showing the superior performance of water-dispersible nanocatalysts at low regeneration temperatures. To further evaluate the effect of water-dispersible nanocatalysts, the CO_2 desorption enhancement achieved after adding Fe_3O_4 -Ala-C was calculated at different time intervals (Figure 3d). It was found that the optimum catalytic activity was obtained after 10 min, which corresponds to a 65 °C regeneration temperature, leading to ~207% enhancement in the CO_2 desorption rate. This confirms the direct relationship between the operating temperature and the rate of CO_2 desorption during the first 20 min of operation until 65 °C and a reduction in catalytic activity at higher temperatures. The increase in the rate of CO_2 desorption can significantly increase the total amount of CO_2 molecules desorbed from the solvent. For instance, the blank solvent released ~204.7 mmol CO_2 during ~20 min solvent regeneration, whereas a higher value of 334.3 mmol was recorded at the same regeneration conditions (approximately 63% more) when Fe_3O_4 -Ala-C was added to the solvent (Figure 3e). This improvement in CO_2 desorption can effectively compensate for the lower regeneration temperature

at 88 °C, compared to the general solvent regeneration temperature at 120–140 °C, and pave the way for using hot water in industrial CO_2 absorption–desorption processes.

To display the superiority of water-dispersible Fe_3O_4 nanocatalysts for low-temperature solvent regeneration, the relative heat duty of CO_2 -saturated 5 M MEA solvent with Fe_3O_4 -Ala-C nanocatalyst was compared with those of typical heterogeneous solid acid catalysts (i.e., Al_2O_3 and HZSM-5) and effective nanocomposite materials ($\text{SO}_4^{2-}/\text{ZrO}_2/\text{Al}_2\text{O}_3$ and $\text{SO}_4^{2-}/\text{ZrO}_2/\text{SBA}-15$). According to Figure 3f, both Al_2O_3 and HZSM-5 exhibited a negligible reduction in relative heat duty (~3.4–3.8%) throughout the regeneration of CO_2 -rich amine solution owing to their very low concentration (0.1 wt %). As previously reported, a higher concentration of heterogeneous catalysts (e.g., 1.25 wt % for Al_2O_3 /HZSM-5⁴² and 5 wt % for montmorillonite²⁵) is needed to effectively observe the catalytic activity of heterogeneous materials. The $\text{SO}_4^{2-}/\text{ZrO}_2/\text{Al}_2\text{O}_3$ and $\text{SO}_4^{2-}/\text{ZrO}_2/\text{SBA}-15$ catalysts exhibited a relative heat duty of 89.8 and 86.1%, respectively, which were much better than those of other well-known heterogeneous catalysts (e.g., Al_2O_3 and HZSM-5). However, the range of performance for these materials is not compelling enough, particularly when comparing the results with those of water-dispersible nanocatalyst. In contrast, the presence of Fe_3O_4 -Ala-C exhibited a relative heat duty of 60.2%, which was ~10-fold better than those of heterogeneous solid acid catalysts at the same concentration, mainly due to the high accessibility of hydrophilic nanocatalysts in the aqueous solvent, their nanofluidic behavior, and the unique decoration of acidic functional groups on the surface of the water-dispersible nanocatalyst. Importantly, the Fe_3O_4 -Ala-C indicated good recyclability with only ~7.7% decrease in its catalytic activity (relative heat duty increased from 60.2 to 67.9) during the first three CO_2 absorption–desorption cycles (i.e., reduction period) and remained nearly stable in the rest seven cycles (i.e., stabilization period) (Figure 3g). In addition,

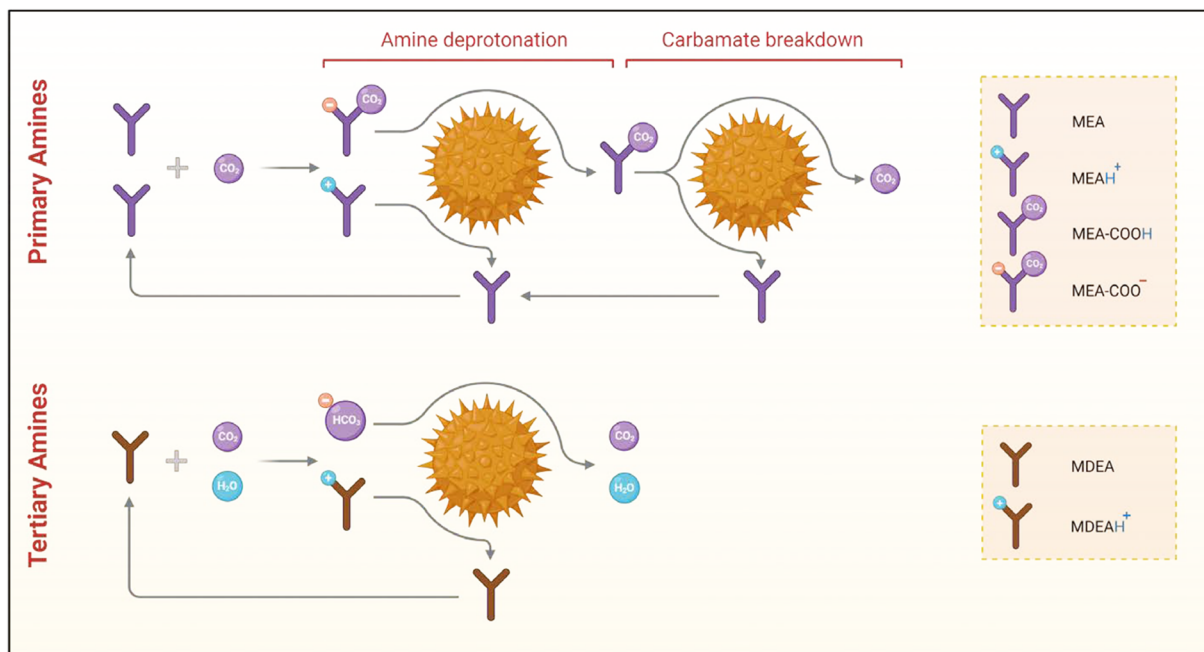


Figure 5. Proposed reaction mechanism for the low-temperature solvent regeneration in the presence of a nanocatalyst.

the recycled Fe_3O_4 -Ala-C after cyclic CO_2 absorption–desorption operation displayed no significant changes in their TEM images and EDX elemental mappings, reconfirming the acceptable recyclability of water-dispersible nanocatalysts (Figure S12).

3.4. Promotion Mechanism in Different Aqueous Solvents. Amino acids have been identified as environmentally friendly substitutes for alkanolamines, owing to the same amine functional group in their molecular structures. Here, we examined the catalytic performance of water-dispersible Fe_3O_4 -Ala-C in a series of amino acid solutions, including long-chain (i.e., arginine and lysine), short-chain (i.e., glycine and sarcosine) and cyclic (i.e., histidine) amino acids. The Fe_3O_4 -Ala-C nanocatalyst successfully enhanced the rate of CO_2 desorption in all the amino acid solutions, depending on their physical-chemical properties, such as the number of amine functional groups, pK_a values, molecular weight and water solubility. For example, Fe_3O_4 -Ala-C displayed lower catalytic activity in both arginine and lysine solutions, with 67.4% and 60.6% relative heat duty, respectively, than the similar amounts recorded for glycine (60.4%) and sarcosine (57.9%) solutions (Figure 4a). This could be attributed to the higher number of amino groups in long-chain amino acids (two or more per molecule) compared to the single amine functional group in the short-chain amino acids. It was also found that the histidine solution has the minimum relative heat duty of 46.3% in the presence of Fe_3O_4 -Ala-C nanocatalyst, which may be because of its phase-change behavior and crystal formation after CO_2 absorption (Figure S13). CO_2 -containing species, obtained by chemical reactions between histidine and CO_2 molecules, have a low solubility in aqueous solutions, resulting in solid precipitation. The accumulation of CO_2 -containing species in the solid phase could provide a better interaction between the nanocatalyst and its targeted molecules. Based on these promising findings, the role of acidic catalysts (either heterogeneous or water-

dispersible) in aqueous amino acid solutions should be further explored in future studies.

To elucidate the reaction mechanism in catalytic solvent regeneration process, the performance of Fe_3O_4 -Ala-C was investigated in different amine solutions, including MEA (i.e., primary amine), MDEA (i.e., tertiary amine) and their mixtures (i.e., MEA-MDEA). The amount of required energy for the regeneration of MDEA without using nanocatalyst was ~10% less than that of MEA (Figure 4b). After mixing MEA and MDEA, the relative heat duty of regeneration significantly reduced to 59.2%, which was much less than those of MEA (100%) and MDEA (90.2%), separately. This energy reduction with no catalyst provides a superior infrastructure to further decrease the required amount of energy using water-dispersible nanocatalysts. As a result, MDEA and MEA-MDEA solutions were regenerated with only 38.6% and 24.6% relative heat duty, respectively, in the presence of 0.1 wt % Fe_3O_4 -Ala-C nanocatalyst, while a substantially higher value of 57.6% was recorded for MEA in similar conditions. This observation could be justified by the synergistic effect between tertiary amines and acidic nanocatalysts throughout the course of CO_2 desorption reactions. According to the widely accepted zwitterion mechanism, which considers carbamate breakdown and amine deprotonation as the main endothermic CO_2 desorption reactions, the difficulty of proton transfer from protonated amines (e.g., MEA^+) to carbamate molecules (e.g., MEACOO^-) is the main challenge for the low-temperature regeneration of primary amines.²² On the other hand, CO_2 molecules are mainly stored in the form of bicarbonate (HCO_3^-) after being absorbed in tertiary amines (e.g., MDEA) without any carbamate formation (Figures 5 and S14). Since HCO_3^- is a better proton acceptor/donor than water molecules, using a MEA-MDEA mixture, and consequently the presence of HCO_3^- during the regeneration of primary amine solutions, can facilitate the proton transfer from protonated amines (e.g., MEA^+) to carbamate molecules and

accelerate the release of CO₂ through a carbamate formation reaction at low temperatures.⁴³

The superior proton transfer ability of water-dispersible nanocatalysts is due to the high density of acidic functional groups (containing both carboxylates and sulfates) as Brønsted acid sites and the metal-oxide itself with Lewis acid sites. In addition, the presence of acidic functional groups on the surface can remarkably increase the hydrophilicity of nanocatalysts and enhance their stability and dispersion in the aqueous solutions by providing hydrogen bonds between the water molecules and their surface. Hence, water-dispersible nanocatalysts could exhibit nanofluidic behavior in the aqueous solutions with positive effects on mass transfer coefficients in CO₂ absorption and desorption processes (as reported by previous studies²¹), resulting in higher CO₂ absorption/desorption rates and less energy consumption. To experimentally support this statement, we measured the CO₂ desorption performance of the conventional Fe₃O₄ nanoparticles (without any surface functionalization). The results indicated that the presence of conventional Fe₃O₄ nanoparticles during the regeneration of 5 M MEA can only reduce the amount of energy required by ~5.3%, which is much less than that of water-dispersible Fe₃O₄-Ala and Fe₃O₄-Ala-C at the same operating conditions (Figure S15). It confirms the determining role of acidic surface functionalization on the nanofluidic and catalytic behavior of water-dispersible nanocatalysts. Therefore, the unique combination of both physical and chemical promotion effects can justify the excellent catalytic performance of water-dispersible nanocatalysts.

4. CONCLUSIONS

We introduced a new strategy for energy-efficient CO₂ absorption–desorption using water-dispersible Fe₃O₄ nanomaterials with high dispersibility and proton donation ability in aqueous solutions. The hydrophilic nanocatalysts were prepared using a simple and environmentally friendly methodology in an aqueous solution and engineered through a one-pot synthesis without further postmodification. The resulting materials exhibited excellent catalytic performance in the aqueous solution of different amines and amino acids, which is attributed to their hydrophilic nature, nanofluid behavior, and Brønsted acidic sites. We also suggested a new plant design with a simpler process configuration and lower investment cost, in which the regeneration column and its high-temperature reboiler can be replaced by a liquid–gas phase separator and liquid–liquid heat exchanger, enabling the process to operate with solar hot water as the main source of energy. We anticipate that the current water-dispersible nanocatalysts, along with their simple process operation, will pave the way for utilizing sustainable energy resources for low-temperature solvent regeneration and open up a new avenue for developing advanced catalytic CO₂ capture processes.

■ ASSOCIATED CONTENT

SI Supporting Information

The Supporting Information is available free of charge at <https://pubs.acs.org/doi/10.1021/acsami.1c17678>.

Materials preparation methods, data related to the characterization of different prepared materials, CO₂ desorption experiments, and reaction mechanisms (PDF)

■ AUTHOR INFORMATION

Corresponding Author

Kathryn A. Mumford – Department of Chemical Engineering, The University of Melbourne, Parkville, Victoria 3010, Australia;  orcid.org/0000-0002-7056-5600; Email: mumfordk@unimelb.edu.au; Fax: +61-3-83444153

Authors

Masood S. Alivand – Department of Chemical Engineering, The University of Melbourne, Parkville, Victoria 3010, Australia;  orcid.org/0000-0002-3391-914X

Omid Mazaheri – Department of Chemical Engineering, The University of Melbourne, Parkville, Victoria 3010, Australia; School of Agriculture and Food, Faculty of Veterinary and Agricultural Sciences, The University of Melbourne, Parkville, Victoria 3010, Australia;  orcid.org/0000-0002-9749-9842

Yue Wu – Department of Chemical Engineering, The University of Melbourne, Parkville, Victoria 3010, Australia;  orcid.org/0000-0001-8592-0460

Ali Zavabeti – Department of Chemical Engineering, The University of Melbourne, Parkville, Victoria 3010, Australia;  orcid.org/0000-0002-5860-8938

Geoffrey W. Stevens – Department of Chemical Engineering, The University of Melbourne, Parkville, Victoria 3010, Australia;  orcid.org/0000-0002-5788-4682

Colin A. Scholes – Department of Chemical Engineering, The University of Melbourne, Parkville, Victoria 3010, Australia;  orcid.org/0000-0002-3810-2251

Complete contact information is available at:
<https://pubs.acs.org/10.1021/acsami.1c17678>

Notes

The authors declare no competing financial interest.

■ REFERENCES

- (1) Wei, Y.-M.; Kang, J.-N.; Liu, L.-C.; Li, Q.; Wang, P.-T.; Hou, J.-J.; Liang, Q.-M.; Liao, H.; Huang, S.-F.; Yu, B. A Proposed Global Layout of Carbon Capture and Storage in Line with a 2 °C Climate Target. *Nat. Clim. Change* **2021**, *11* (2), 112–118.
- (2) Samset, B. H.; Fuglestvedt, J. S.; Lund, M. T. Delayed Emergence of a Global Temperature Response after Emission Mitigation. *Nat. Commun.* **2020**, *11* (1), 3261.
- (3) Smith, C. J.; Forster, P. M.; Allen, M.; Fuglestvedt, J.; Millar, R. J.; Rogelj, J.; Zickfeld, K. Current fossil Fuel Infrastructure Does Not yet Commit Us to 1.5 °C Warming. *Nat. Commun.* **2019**, *10* (1), 101.
- (4) Forster, E. J.; Healey, J. R.; Dymond, C.; Styles, D. Commercial Afforestation Can Deliver Effective Climate Change Mitigation under Multiple Decarbonisation Pathways. *Nat. Commun.* **2021**, *12* (1), 3831.
- (5) Realmonte, G.; Drouet, L.; Gambhir, A.; Glynn, J.; Hawkes, A.; Köberle, A. C.; Tavoni, M. An Inter-Model Assessment of the Role of Direct Air Capture in Deep Mitigation Pathways. *Nat. Commun.* **2019**, *10* (1), 3277.
- (6) Alivand, M. S.; Mazaheri, O.; Wu, Y.; Stevens, G. W.; Scholes, C. A.; Mumford, K. A. Development of Aqueous-Based Phase Change Amino Acid Solvents for Energy-Efficient CO₂ Capture: The Role of Antisolvent. *Appl. Energy* **2019**, *256*, 113911.
- (7) Alivand, M. S.; Mazaheri, O.; Wu, Y.; Stevens, G. W.; Scholes, C. A.; Mumford, K. A. Preparation of Nanoporous Carbonaceous Promoters for Enhanced CO₂ Absorption in Tertiary Amines. *Engineering* **2020**, *6* (12), 1381–1394.
- (8) Wu, Y.; Alivand, M. S.; Hu, G.; Stevens, G. W.; Mumford, K. A. Nucleation Kinetics of Glycine Promoted Concentrated Potassium

- Carbonate Solvents for Carbon Dioxide Absorption. *Chem. Eng. J.* **2020**, *381*, 122712.
- (9) Kirchner, J. S.; Berry, A.; Ohnemüller, F.; Schnetger, B.; Erich, E.; Brumsack, H.-J.; Lettmann, K. A. Reducing CO₂ Emissions of a Coal-Fired Power Plant Via Accelerated Weathering of Limestone: Carbon Capture Efficiency and Environmental Safety. *Environ. Sci. Technol.* **2020**, *54* (7), 4528–4535.
- (10) Alivand, M. S.; Shafei-Alavijeh, M.; Tehrani, N. H. M. H.; Ghasemy, E.; Rashidi, A.; Fakhraie, S. Facile and High-Yield Synthesis of Improved MIL-101(Cr) Metal-Organic Framework with Exceptional CO₂ and H₂S Uptake; the Impact of Excess Ligand-Cluster. *Microporous Mesoporous Mater.* **2019**, *279*, 153–164.
- (11) Sheikh Alivand, M.; Hossein Tehrani, N. H. M.; Shafei-alavijeh, M.; Rashidi, A.; Kooti, M.; Pourreza, A.; Fakhraie, S. Synthesis of a Modified Hf-Free MIL-101(Cr) Nanoadsorbent with Enhanced H₂S/CH₄, CO₂/CH₄, and CO₂/N₂ Selectivity. *J. Environ. Chem. Eng.* **2019**, *7* (2), 102946.
- (12) Saifdarnejad, S. M.; Hedengren, J. D.; Baxter, L. L. Plant-Level Dynamic Optimization of Cryogenic Carbon Capture with Conventional and Renewable Power Sources. *Appl. Energy* **2015**, *149*, 354–366.
- (13) Song, C.; Liu, Q.; Deng, S.; Li, H.; Kitamura, Y. Cryogenic-Based CO₂ Capture Technologies: State-of-the-Art Developments and Current Challenges. *Renewable Sustainable Energy Rev.* **2019**, *101*, 265–278.
- (14) Legrand, L.; Schaetzle, O.; de Kler, R. C. F.; Hamelers, H. V. M. Solvent-Free CO₂ Capture Using Membrane Capacitive Deionization. *Environ. Sci. Technol.* **2018**, *52* (16), 9478–9485.
- (15) Fan, S.-T.; Qiu, Z.-J.; Xu, R.-Y.; Zhang, S.-X.; Chen, Z.-H.; Nie, Z.-J.; Shu, H.-R.; Guo, K.; Zhang, S.; Li, B.-J. Ultrahigh Carbon Dioxide-Selective Composite Membrane Containing a Γ -Cd-Mof Layer. *ACS Appl. Mater. Interfaces* **2021**, *13* (11), 13034–13043.
- (16) Mumford, K. A.; Wu, Y.; Smith, K. H.; Stevens, G. W. Review of Solvent Based Carbon-Dioxide Capture Technologies. *Front. Chem. Sci. Eng.* **2015**, *9* (2), 125–141.
- (17) Bhatti, U. H.; Shah, A. K.; Hussain, A.; Khan, H. A.; Park, C. Y.; Nam, S. C.; Baek, I. H. Catalytic Activity of Facilely Synthesized Mesoporous HZSM-5 Catalysts for Optimizing the CO₂ Desorption Rate from CO₂-Rich Amine Solutions. *Chem. Eng. J.* **2020**, *389*, 123439.
- (18) Bhatti, U. H.; Sultan, H.; Min, G. H.; Nam, S. C.; Baek, I. H. Ion-Exchanged Montmorillonite as Simple and Effective Catalysts for Efficient CO₂ Capture. *Chem. Eng. J.* **2021**, *413*, 127476.
- (19) Lai, Q.; Toan, S.; Assiri, M. A.; Cheng, H.; Russell, A. G.; Adidharma, H.; Radosz, M.; Fan, M. Catalyst-TiO(OH)₂ Could Drastically Reduce the Energy Consumption of CO₂ Capture. *Nat. Commun.* **2018**, *9* (1), 2672.
- (20) Zhang, S.; Shen, Y.; Wang, L.; Chen, J.; Lu, Y. Phase Change Solvents for Post-Combustion CO₂ Capture: Principle, Advances, and Challenges. *Appl. Energy* **2019**, *239*, 876–897.
- (21) Yu, W.; Wang, T.; Park, A.-H. A.; Fang, M. Review of Liquid Nano-Absorbents for Enhanced CO₂ Capture. *Nanoscale* **2019**, *11* (37), 17137–17156.
- (22) Alivand, M. S.; Mazaheri, O.; Wu, Y.; Stevens, G. W.; Scholes, C. A.; Mumford, K. A. Catalytic Solvent Regeneration for Energy-Efficient CO₂ Capture. *ACS Sustainable Chem. Eng.* **2020**, *8* (51), 18755–18788.
- (23) Bhatti, U. H.; Nam, S.; Park, S.; Baek, I. H. Performance and Mechanism of Metal Oxide Catalyst-Aided Amine Solvent Regeneration. *ACS Sustainable Chem. Eng.* **2018**, *6* (9), 12079–12087.
- (24) Bhatti, U. H.; Shah, A. K.; Kim, J. N.; You, J. K.; Choi, S. H.; Lim, D. H.; Nam, S.; Park, Y. H.; Baek, I. H. Effects of Transition Metal Oxide Catalysts on MEA Solvent Regeneration for the Post-Combustion Carbon Capture Process. *ACS Sustainable Chem. Eng.* **2017**, *5* (7), 5862–5868.
- (25) Bhatti, U. H.; Kazmi, W. W.; Muhammad, H. A.; Min, G. H.; Nam, S. C.; Baek, I. H. Practical and Inexpensive Acid-Activated Montmorillonite Catalysts for Energy-Efficient CO₂ Capture. *Green Chem.* **2020**, *22* (19), 6328–6333.
- (26) Xing, L.; Wei, K.; Li, Q.; Wang, R.; Zhang, S.; Wang, L. One-Step Synthesized SO₄²⁻/ZrO₂-HZSM-5 Solid Acid Catalyst for Carbamate Decomposition in CO₂ Capture. *Environ. Sci. Technol.* **2020**, *54* (21), 13944–13952.
- (27) Zhang, X.; Zhu, Z.; Sun, X.; Yang, J.; Gao, H.; Huang, Y.; Luo, X.; Liang, Z.; Tontiwachwuthikul, P. Reducing Energy Penalty of CO₂ Capture Using Fe Promoted SO₄²⁻/ZrO₂/MCM-41 Catalyst. *Environ. Sci. Technol.* **2019**, *53* (10), 6094–6102.
- (28) Xing, L.; Wei, K.; Li, Y.; Fang, Z.; Li, Q.; Qi, T.; An, S.; Zhang, S.; Wang, L. TiO₂ Coating Strategy for Robust Catalysis of the Metal-Organic Framework toward Energy-Efficient CO₂ Capture. *Environ. Sci. Technol.* **2021**, *55* (16), 11216–11224.
- (29) Gao, H.; Huang, Y.; Zhang, X.; Bairq, Z. A. S.; Huang, Y.; Tontiwachwuthikul, P.; Liang, Z. Catalytic Performance and Mechanism of SO₄²⁻/ZrO₂/SBA-15 Catalyst for CO₂ Desorption in CO₂-Loaded Monoethanolamine Solution. *Appl. Energy* **2020**, *259*, 114179.
- (30) Zhang, X.; Zhang, X.; Liu, H.; Li, W.; Xiao, M.; Gao, H.; Liang, Z. Reduction of Energy Requirement of CO₂ Desorption from a Rich CO₂-Loaded MEA Solution by Using Solid Acid Catalysts. *Appl. Energy* **2017**, *202*, 673–684.
- (31) Ali Saleh Bairq, Z.; Gao, H.; Huang, Y.; Zhang, H.; Liang, Z. Enhancing CO₂ Desorption Performance in Rich MEA Solution by Addition of SO₄²⁻/ZrO₂/SiO₂ Bifunctional Catalyst. *Appl. Energy* **2019**, *252*, 113440.
- (32) Far, H. S.; Hasanzadeh, M.; Nashtaei, M. S.; Rabbani, M.; Haji, A.; Hadavi Moghadam, B. Ppi-Dendrimer-Functionalized Magnetic Metal-Organic Framework (Fe₃O₄@Mof@Ppi) with High Adsorption Capacity for Sustainable Wastewater Treatment. *ACS Appl. Mater. Interfaces* **2020**, *12* (22), 25294–25303.
- (33) Chen, R.; Tao, C.-a.; Zhang, Z.; Chen, X.; Liu, Z.; Wang, J. Layer-by-Layer Fabrication of Core-Shell Fe₃O₄@UiO-66-NH₂ with High Catalytic Reactivity toward the Hydrolysis of Chemical Warfare Agent Simulants. *ACS Appl. Mater. Interfaces* **2019**, *11* (46), 43156–43165.
- (34) Gschneidtner, T. A.; Lerch, S.; Olsén, E.; Wen, X.; Liu, A. C. Y.; Stolář, A.; Etheridge, J.; Olsson, E.; Moth-Poulsen, K. Constructing a Library of Metal and Metal-Oxide Nanoparticle Heterodimers through Colloidal Assembly. *Nanoscale* **2020**, *12* (20), 11297–11305.
- (35) Zhang, Z.; Cai, J.; Chen, F.; Li, H.; Zhang, W.; Qi, W. Progress in Enhancement of Co₂ Absorption by Nanofluids: A Mini Review of Mechanisms and Current Status. *Renewable Energy* **2018**, *118*, 527–535.
- (36) Lee, A. F.; Bennett, J. A.; Manayil, J. C.; Wilson, K. Heterogeneous Catalysis for Sustainable Biodiesel Production Via Esterification and Transesterification. *Chem. Soc. Rev.* **2014**, *43* (22), 7887–7916.
- (37) Song, H.; Xing, C.; Li, B.; Shen, W. Spherical Carbon with SO₃H Groups as an Efficient Solid Acid Catalyst for 2,4,5-Triphenyl-Imidazole Synthesis. *ChemistrySelect* **2016**, *1* (2), 301–308.
- (38) Nakajima, K.; Hara, M. Amorphous Carbon with SO₃H Groups as a Solid Brønsted Acid Catalyst. *ACS Catal.* **2012**, *2* (7), 1296–1304.
- (39) Bhatti, U. H.; Sivanesan, D.; Nam, S.; Park, S. Y.; Baek, I. H. Efficient Ag₂O-Ag₂CO₃ Catalytic Cycle and Its Role in Minimizing the Energy Requirement of Amine Solvent Regeneration for CO₂ Capture. *ACS Sustainable Chem. Eng.* **2019**, *7* (12), 10234–10240.
- (40) Zhang, X.; Huang, Y.; Gao, H.; Luo, X.; Liang, Z.; Tontiwachwuthikul, P. Zeolite Catalyst-Aided Tri-Solvent Blend Amine Regeneration: An Alternative Pathway to Reduce the Energy Consumption in Amine-Based CO₂ Capture Process. *Appl. Energy* **2019**, *240*, 827–841.
- (41) Zhang, X.; Huang, Y.; Yang, J.; Gao, H.; Huang, Y.; Luo, X.; Liang, Z.; Tontiwachwuthikul, P. Amine-Based CO₂ Capture Aided by Acid-Basic Bifunctional Catalyst: Advancement of Amine Regeneration Using Metal Modified MCM-41. *Chem. Eng. J.* **2020**, *383*, 123077.
- (42) Zhang, X.; Liu, H.; Liang, Z.; Idem, R.; Tontiwachwuthikul, P.; Jaber Al-Marri, M.; Benamor, A. Reducing Energy Consumption of

CO₂ Desorption in CO₂-Loaded Aqueous Amine Solution Using Al₂O₃/HZSM-5 Bifunctional Catalysts. *Appl. Energy* **2018**, *229*, 562–576.

(43) Zhang, X.; Zhang, R.; Liu, H.; Gao, H.; Liang, Z. Evaluating CO₂ Desorption Performance in CO₂-Loaded Aqueous Tri-Solvent Blend Amines with and without Solid Acid Catalysts. *Appl. Energy* **2018**, *218*, 417–429.